

# Large Scale Earth's Bow Shock with Northern IMF as simulated by PIC code in parallel with MHD model

Suleiman M Baraka<sup>(1,2,3)</sup>

April 4, 2016

<sup>(1)</sup> Faculty in residence, National Institute of Aerospace,  
100, Exploration Way Hampton, VA  
suleiman.baraka@nianet.org

<sup>(2)</sup> Center for Astronomy and Space Sciences-CASSR.  
Al Aqsa University, P.O.Box 4051, Gaza, Palestine.  
suleiman.baraka@gmail.com

<sup>(3)</sup> Institut d'Astrophysique de Paris  
98 bis Blvd Arago, 75015, Paris, France  
baraka@iap.fr

## Abstract

In this paper, we propose a 3D kinetic model (Particle-in-Cell PIC) for the description of the large scale Earth's bow shock. The proposed version is stable and does not require huge or extensive computer resources. Because PIC simulations work with scaled plasma and field parameters, we also propose to validate our code by comparing its results with the available MHD simulations under same scaled Solar wind (SW) and (IMF) conditions. We report new results from the two models. In both codes the Earth's bow shock position is found to be  $\approx 14.8R_E$  along the Sun-Earth line, and  $\approx 29R_E$  on the dusk side. Those findings are consistent with past in situ observations. Both simulations reproduce the theoretical jump conditions at the shock. However, the PIC code density and temperature distributions are inflated and slightly shifted sunward when compared to the MHD results. Kinetic electron motions and reflected ions upstream may cause this sunward shift. Species distributions in the foreshock region are depicted within the transition of the shock (measured  $\approx 2 c/\omega_{pi}$  for  $\Theta_{Bn} = 90^\circ$  and  $M_{MS} = 4.7$ ) and in the downstream. The size of the foot jump in the magnetic field at the shock is measured to be  $(1.7c/\omega_{pi})$ . In the foreshocked region, the thermal velocity is found equal to  $213 \text{ km}\cdot\text{sec}^{-1}$  at  $15R_E$  and is equal to  $63 \text{ km}\cdot\text{sec}^{-1}$  at  $12 R_E$  (Magnetosheath region). Despite the large cell size of the current version of the PIC code, it is powerful to retain macrostructure of planets magnetospheres in very short time, thus it can be used for a pedagogical test purposes. It is also likely complementary with MHD to deepen our understanding of the large scale magnetosphere

# 1 Introduction

Shocks in astrophysical systems are mainly non-relativistic shocks (relativistic shocks are not in the reach of man-made spacecraft). They have widths of order of the ion inertial length ( $c/\omega_{pi}$ ) or ion gyro-radius ( $v_{\perp}/\omega_{ci}$  i.e. resistive scale  $\sim 10^{-6}$  mean free path). The collisionless astrophysical shocks is important to understand their effects in dissipating flow-energy, in heating matter, in accelerating particles to high presumably cosmic-ray energies, and in generating detectable radiation from radio to X-rays.<sup>16,61</sup>.

The Earth's bow shock was proposed by Axford<sup>1</sup> and<sup>32</sup>, since then many theoretical and statistical studies based on space observations have been conducted to study its position and shape for a large set of upstream solar wind plasma and field conditions<sup>22,27,30,31,39,40,42,52</sup>. On the other hand, there are many approaches to study the bow shock location, dynamics and physical properties, such as Hybrid models<sup>24,46,55</sup>, MHD models<sup>33,56,60,64</sup>, and PIC models<sup>(4,57,58,62)</sup> and the references therein.

Leboeuf et al.<sup>37</sup> was the first to use MHD modeling of the global interaction of the magnetosphere with the solar wind. Over the years these models have increased greatly in their sophistication and scope<sup>28</sup>. The MHD use only ensemble-averaged parameters which assume the distribution of the particles velocity as a collection of several Maxwellian functions as in<sup>65</sup>. Under the influence of the magnetic field where velocity distributions along and across the field lines are generally different, these calculations do not determine the plasma microphysics<sup>11,35,41,50,59</sup>. On the other hand, the ideal MHD theory may removes the capability for the plasma to act electromagnetically. This restriction severely limits the kind of physics one can do with ideal fluid<sup>49</sup>.

Our code (modified from Buneman et al.<sup>14</sup>) is a PIC code. Global PIC EM code has severe constraints on spatial and temporal scales despite it contained more physics than explicitly assuming Ohm's law. The most limiting of them are  $\Delta x < \lambda_{De}$ ,  $c\Delta t < \Delta x/\sqrt{n}$  and  $\omega_{pe}\Delta t < 2$ , where  $\Delta x$  is the grid size,  $\Delta t$  is the time step and  $\omega_{pe}$  is the electron plasma frequency. However, this method is superior to MHD simulation in some aspects such as in modeling kinetic processes that separate the electrons and ions dynamics<sup>44,66,19</sup>. For instance, MHD has no fundamental

length scale in contrast with PIC simulations for which a gyro-radius can be derived for particles despite the limitation on the  $\frac{m_i}{m_e}$  mass ratio.

In this paper, a Particle-In-Cell PIC is used for the description of Earth's bow shock. The proposed version is stable and does not require huge or expensive computer resources since we are interested in the large scales of the system ( $1R_E$ )<sup>5</sup>. The scaled plasmas and fields parameters used in PIC, was also used to validate our code with available MHD simulations.

## 2 Simulation Models

In this section a brief introduction of PIC-EM and MHD-GUMICS models is presented. As in our previous work<sup>5</sup>, the current version of the code is capable to form the macrostructure of the Earth's magnetosphere. The MHD model is introduced based on the CCMC requested run ([http://ccmc.gsfc.nasa.gov/results/viewrun.php?domain=GM&runnumber=Suleiman\\_Baraka\\_112610\\_2](http://ccmc.gsfc.nasa.gov/results/viewrun.php?domain=GM&runnumber=Suleiman_Baraka_112610_2)). GUMICS-v4 details are also available at Janhunen et al.<sup>29</sup>.

### 2.1 PIC EM Relativistic Global Code

In our simulation, we use the same initial conditions in<sup>12-15</sup> to generate the macrostructure of the magnetosphere. The radiating boundary conditions is adopted as in<sup>38</sup> and for the charge description inside the box we used the charge-conserving formulas reported by<sup>63</sup>. The same initial and boundary conditions were also used in our previous work<sup>4-9</sup>. The grid size in the simulation should take into account the nonphysical instabilities. In our simulation, they are taken care of by Courant Condition ( $\delta x, \delta y, \delta z > c\delta t$ ), which satisfies the inequality  $\frac{\lambda_{Dei}}{\delta x} > \frac{1}{\pi}$ <sup>10</sup>.

Pritchett<sup>54</sup> thoroughly discussed cons and pros of formulating PIC codes for space simulation. Whilst Parks<sup>49</sup> clearly stated that understanding collisionless plasma dynamics requires self-consistent Particle-In-Cell kinetic modeling. The spatial dimensions of the 3D EM global code used in this simulation is set such that OX is pointing from Earth to Sun, OY toward dusk direction and OZ toward north direction. The dimension of the simulation box is taken equal to  $(155\Delta \times 105\Delta \times 105\Delta)$ , where the grid size  $\Delta = \Delta x = \Delta y = \Delta z = 1R_E$  and  $\Delta t$  is the time step ( $\omega_{pe}\Delta t = 0.22$ ). The simulation box is uniformly filled up by  $2 \times 10^6$  of equal electrons-ions

pairs, this number is equivalent to a uniform particle density of  $n_e = n_i = \frac{N}{\Delta^3} = 0.8$  pairs per cell.

The physical parameters (normalized) used in our simulation as pairs of numbers (unitless values for electrons and ions) are as follow, the gyro-frequencies are  $\tilde{\omega}_{ce,i} = \omega_{ce,i}\Delta t = (0.2, 0.0125)$ , the thermal velocities for the two species are  $\tilde{v}_{the,i} = v_{the,i}/(\Delta/\Delta t) = (0.1, 0.025) = (B\Delta m_e/\Delta t m_{e,i})$ , the Debye length is  $\lambda_{De,i} = \tilde{v}_{the,i}/\tilde{\omega}_{pe,i} = (0.11, 0.11)$ , Larmour gyro-radii are  $\tilde{\rho}_{ce,i} = \tilde{v}_{the,i}/\tilde{\omega}_{ce,i} = (1.25, 20)$ , inertial lengths are  $\tilde{\lambda}_{e,i} = \tilde{c}/\tilde{\omega}_{pe,i} = (0.559, 2.236)$ . The impinged drift velocity of the solar wind along the Sun-Earth line is  $V_{sw} = -0.25 = 0.5\tilde{c}$ , where the speed of light's normalized value is taken  $\tilde{c} = 0.5$ , the ion to mass ratio is  $m_i/m_e = 16$ . The Normalized magnetic field is  $\tilde{B} = \vec{B}(\frac{q(\Delta t)^2}{m_e \Delta})$ , the IMF is northward  $B_z(x) = 0.2$ , the  $\beta_{e,i} = (1.6, 6.4)$ . The normalized ion temperature is  $\tilde{T}_i = \tilde{v}_{thi}^2 m_i = 0.04$ , and for electrons the temperature is  $\tilde{T}_e = \tilde{v}_{the}^2 m_e = 0.01$ , where the "e" and the "i" denotes electrons and ions respectively. On the other hand, Our code was run until it reached a steady state at time step  $900\Delta t$ , where  $\Delta t$  is the numerical time step<sup>3,5</sup>. Moreover in the PIC simulation, the macroscopic bulk properties of the flow are,  $V_A = 0.027$ ,  $\frac{V_A}{V_{sw}} = 0.11$ ,  $M_A = 9.219$ ,  $M_S = 2.858$ ,  $M_{MS} = 2.730$ , Plasma parameters were then derived and scaled so that the flow input conditions are used to simulate the same case study by MHD model.

## 2.2 MHD model: GUMICS

The Community Coordinated Modeling Center (CCMC) is a multi-agency partnership. The CCMC provides, to the international research community, access to modern space science simulations. In addition, the CCMC supports the transition to space weather operations of modern space research models. More information about CCMC can be found here (<http://ccmc.gsfc.nasa.gov/>)

GUMICS is a global solar wind-magnetosphere-ionosphere coupling model. Its solar wind and magnetospheric part is based on solving the ideal MHD equations and its ionosphere part is based on solving the electrostatic current continuity equation. Advanced numerical methods such as automatically refined Cartesian octogrid and temporal sub-cycling are used to speed up the computation. The computational box dimension is taken from  $-224$  to  $+32 R_E$  in *GSE X* and

from  $-64$  to  $+64 R_E$  in  $Y$  and  $Z$  [<sup>36,47,48</sup>, official website is here (<http://ccmc.gsfc.nasa.gov/models/modelinfo.php?model=GUMICS>)].

The inflow boundary conditions are carried out in 5 hours, and the dipole tilt in GSE coordinates is taken to be zero. The initial solar wind velocity is  $V_{sw}(x) = -500\text{km}\cdot\text{sec}^{-1}$ , the solar wind density is  $\rho_{sw} = 5.0\text{N}\cdot\text{cm}^{-3}$ . The solar wind temperature is  $T_{e,i} = 6.7 \times 10^5\text{Kelvin}$ . The initial IMF value in the MHD code was  $B_z = 6.5\text{nT}$  northward oriented. The top level (in terms of hierarchy) of the simulation box has a base grid of  $(8R_E)^3$ . Each cell is broken to 8 sub cells if the refinement exceed a certain limit. The grid size in the magnetohydrodynamics code is changing with the dynamics of the hierarchically adaptive and can reach up to  $0.25 R_E$ <sup>29</sup>.

### 3 Results

The large scale Earth's magnetosphere is simulated by PIC EM relativistic code in parallel with MHD code. One of the key features of both runs is the structure, position and shape of the Earth's bow shock as depicted in the results. The geometry of the Earth's bow shock resembles bullet-like shape(see Fig. 1). Its position was found by both codes to be equal to  $14.9R_E$  as measured along the nose direction from planet position, and  $29.R_E$  along the dusk direction. These results are in good agreement with in situ measurements obtained for  $M_A$  values within the range  $(8 - 13R_E)$  along ( $OX$  direction) as reported by<sup>51</sup>, and shown in Fig ( 2 panel A) and in Fig (3 panel A).

On the other hand, we see in Fig 2 panel (B)) how the velocity simulation of both codes decreases and stagnated at the bow shock position. The simulated velocity by PIC code shows a spatial delay compared to the sharp decrease of the MHD code, seemingly caused by the effect of thermal electrons in the foreshock region (i.e. electrons velocity spatial distribution in Fig 4 panel A & B). Same effect of the velocity profile of both codes can also be seen in Fig (3 panel (B)) in the dusk side. The IMF profile along nose and dusk directions (Fig 2 and 3 panel C) respectively, shows similarities between both codes in the behavior of the magnetic field at the bow shock position.

On the other hand, both temperature profiles in Figs 2 and 3 panel (D) apparently show differences and spatial lags in the temperature jump. This is because in PIC code electrons temperature are included, but not in MHD codes, additionally the thermal velocities of electrons offsets their smaller masses.

To further show similarities and differences between the two codes, the parallel and perpendicular velocity distributions of the PIC code are polar-plotted in Fig 5 panel (A) and for MHD in panel (B). The maximum parallel velocity distribution values is factor 3.4 than that of the perpendicular ones for the PIC code, whilst on the other hand this ratio is factor 2 for the MHD.

On the other hand, If we base our diagnostic on the magnetosonic Mach number  $M_{MS} \approx 5$  in both codes(see Table 1), the above comparison shows that PIC simulation can successfully recover the traditional results of the MHD model in terms of the macrostructure of the bow shock, but at a much lower cost in computational time. Further more to our diagnostic, the

magnetic field (northward input) is shown quasi perpendicularly oriented where it is plotted over the plasma density in Noon-Midnight in Fig 6 panel A, and in Dawn-Dusk direction in 6 panel B.

## 4 Analysis and Discussion

Since the early models of the magnetosphere by<sup>21</sup> through<sup>23</sup> until present, statistical, theoretical, observational, and modeling have been extensively used to comprehensively resolve the magnetospheric unsolved problems.

In our case, we don't re-invent the wheel. Our code development has been considered for upgrade for so many years and still in terms of spatial and temporal resolutions. Additional considerations are given to handle physical instabilities and to reduce CPU run time. In the near future, we will have a validated version of the code that is enhanced in terms of spatial and temporal resolutions with real ion to electron mass ratio. In order to keep the physical problem under investigation fixed, one has to adjust all other physical inputs parameters simultaneously. Because if one changes for example particle density to reduce statistical noises, then all other physical quantities will vary i.e.<sup>18</sup>. This is exactly what has been taken care of in the current case study. The global structure of the collisionless bow shock was investigated by<sup>45</sup>, in their model ions are treated kinetically, whilst electrons are treated as a massless fluids. It is worth noting that they used 2.5D simulations. Two spatial dimensions and 3D for velocity and currents. Another work consider the magnetosphere simulation by 2.5D was reported by<sup>43</sup>. They reproduce the magnetosphere. In a recent study by<sup>20</sup> a large scale 3D PIC code is used to study the whole terrestrial magnetosphere using ion to electron mass ratio equal to  $\frac{1}{16}$ . In the current study a large scale structure of the magnetosphere was recovered but with full 3D simulations, in addition that electrons kinetics are included in the run. In their simulations and ours as well our physical units were scaled to ion inertial lengths and all were successful to recover the large scale magnetosphere.

However the PIC simulation is not a faithful representation of the plasma physics, it is still a must. On the other hand, even with the huge super-computing facilities available nowadays, it

is quite impossible to simulate real magnetosphere. Thus scaling is an answer as quoted in the above references. After all these years and all these advances in the magnetospheric physics, we still don't know the magnetosphere(private communication recently with Mikhail Sitnov). One can imagine a cuboid of volume of real magnetosphere equal to  $1.5 \times 10^6$  Earth Radii ( $R_E^3$ ) is considered for simulation while one is looking for kinetic processes that take place in few 10s of meters. In this paper, a macro-structure of the Earth magnetosphere is successfully simulated. It is quite clear that we don't have a High-Definition(HD) image with the current scaled values and their corresponding spatial and temporal resolutions, but, for global structure a little blur image is enough to give a glimpse about the considered physical problem in hand. I think if a comprehensive answer is reached in the space plasma physics field, it would have been enough for the community to pursue the discipline any further. We still on the long road to reach out there. In this section we will analyze the criteria under which the PIC code is used in this study. The MHD code structure, boundary conditions are well defined in Janhunen et al.<sup>29</sup>. Adopting the analysis in<sup>17</sup>, we simulated a dynamic system that include the bow shock in the macroscopic scale, we made sure that our total run time is very much greater than the ion gyroperiod  $\tau_{total} \gg \omega_{ci}^{-1}$ , where  $\omega_{ci}$  is the upstream ion gyro-frequency. Typically the shock thickness is of order of few  $R_E$ , which is very much smaller than the plasma simulation box size.

In Fig 4 panels A and B show the nose and the dusk direction respectively of ions (in blue) and electrons (in red) velocity spatial distribution. In panel A, inflow of ions have relatively small velocity variations before it reached the shock terminal. Whilst on the other hand, the electrons velocity in the dayside spans high variations because of their thermal motions. It is also worth noting the backstreaming of ions and electrons in the foreshock regions. The corresponding velocity spatial distributions in the dawn-dusk directions is shown in panel B.

On the other hand, we measured the velocity (thermal) of ions in the foreshock region (at  $\sim 15R_E$ ) which is found to be equal to  $0.10665$  ( $\approx 213.30 \text{ km.s}^{-1}$ ) and in the Magnetosheath at around  $12R_E$  it is  $0.03150$  ( $\approx 63.0 \text{ km.s}^{-1}$ ), the reference value of solar wind speed is  $0.25$  ( $\approx 500 \text{ km.s}^{-1}$ ). These findings are consistent with the recent study of<sup>53</sup>

Another result we report in the this paper is the magnetic field jump was zoomed in and plotted in the foreshock region Fig 7, where the foot and the ramp of the shock is shown. Overshoot of the shock didn't appear at this current version of the code. This result compared

with analysis of the shock dynamics by<sup>61</sup>. Also another result we report here when the width of the density transition region of the shock was calculated and was found to be  $\approx 2$  ion inertial lengths( $c/\omega_{pi}$ ) as in Fig 8. This result is in full agreement with<sup>2</sup>. This figure is mirror-imaged for comparison reason.

The width of our ramp is  $1.7 c/\omega_{pi} = L_i$ , which is comparable to the value obtained in<sup>34</sup>  $\approx 1.4L_i$ .

However, it is unambiguously established that many observed thinnest ramps are less than  $5c/\omega_{pi}$  thick and there was an apparent trend for lower values as  $\theta_{Bn} \rightarrow 90^0$ . The plasma inertia effects is considered in our PIC simulation, as a consequence the length of the simulation box is very much larger than the Debye length  $\lambda_{Dei}=(0.11, 0.11)$ , the gyro-radius  $\rho_{ce,i}=(1.25, 20)$  and the inertia lengths  $\frac{c}{\omega_{pe,i}} = (5, 80)$  for electrons and ions respectively.

On the other hand, a quick look at Fig 2 ion density jump fact 3, and the foot of the shock clearly appears. A time sequence study of such shocks revealed by PIC, should be carried out in a new paper for deeper verification of these preliminary results, where in Fig 2 the shock is only shown at  $900 \Delta t$ .

It is also worth noting that in Fig 4 the ions and electrons at the upstream of the bow shock, have high velocities, which is consistent with observation<sup>25</sup> and<sup>26</sup>.

One final point is that we can follow the motion of electrons and ions in the self-consistent  $\vec{E}$  and/or  $\vec{B}$  fields obtained from a solution of Maxwell's equations, with relativistic effects are readily included by the use of the Lorentz equation of motion. At this level no approximations in the basic laws of mechanics and electromagnetism is introduced, and thus the full range of collisionless plasma physics is included in such a model<sup>54</sup>, which is the case of the current study.

## 5 Conclusion

The results of this study are summarized as the following:

1. The output data of both runs are retrieved and normalized to input plasma parameters. In this paper, we show distinct features: the bow shock position, jump conditions, plasma density, and fields distributions in specific geometric configurations.
2. Both codes have showed that the bow shock location is found to be at  $\sim 14R_E$  along the Sun-Earth line and at  $\sim 29R_E$  along the dawn-dusk direction, with a factor 3 in density jump. This result is consistent with in situ observations obtained during similar SW and IMF conditions.
3. The (thermal) velocity of ions in the foreshock region (at  $\sim 15R_E$ ) is measured and found to be  $0.10665$  ( $\approx 213.30 \text{ km.s}^{-1}$ ) and its value in the Magnetosheath at around  $12R_E$  is  $0.03150$  ( $\approx 63.0 \text{ km.s}^{-1}$ ), the reference value of solar wind speed is  $0.25$  ( $\approx 500 \text{ km.s}^{-1}$ ).
4. The structure of the magnetic field jump at the shock  $B_z(x)$  of the foot and ramp of the magnetic field is obtained by the PIC code. The width of our ramp is  $1.7 c/\omega_{pi} = L_i$  which is comparable to the value of  $\approx 1.4L_i$ <sup>34</sup>.
5. The density transition between the shocked plasma in the downstream and the unshocked plasma in the upstream is found to be  $\approx 2$  ion inertial length ( $c/\omega_{pi}$ ) at the magnetosonic number 4.7 when  $\Theta_{Bn} = 90^\circ$ .
6. Both simulations reproduce the same basic macroscopic features of the Earth's magnetosphere. However, for the PIC code, a noisy current-sheet naturally appears, but it is absent in the MHD results.
7. The velocity distribution of different species across and parallel the ambient magnetic field can be derived anywhere in the magnetosphere from the PIC simulation, the derivation of that velocity distribution is also absent in MHD results.
8. In PIC models one can follow the motion of electrons and ions in the self-consistent  $\tilde{E}$  and/or  $\tilde{B}$  fields obtained from the solution of Maxwell's equations, with relativistic effects are readily included by the use of the Lorentz equation of motion.

9. In contrast, macroscopic properties of the magnetosphere obtained from MHD simulations can be directly compared to observations, while only scaled quantities from PIC simulations are useful in such comparisons.
10. The results obtained thus far from the present study strongly suggest using MHD and PIC codes in a complementary manner as a new strategy for better understanding of the magnetosphere-solar wind system.
11. The PIC showed the backstreaming velocity distribution of both ions and electrons on the nose and on the dusk-direction in the dayside magnetosphere (foreshock, transition shock, magnetosheath and in the magnetotail).
12. This working version of our PIC code is powerful to simulate large scale magnetospheric electrodynamicics. It is undoubtedly capable of simulating more sophisticated kinetics, such as reconnection, cusp dynamics and current systems if and only if a better computer resources and multiprocessors super computing facilities are available, in order to be able to reduce grid cell size and to increase the number of pair particles of the simulation box.

## 6 acknowledgements

This work would have not been done without the insights and hard work on code development by Dr Lotfi Ben-Jaffel, IAP. I would like also to thank the IAP-CNRS, Paris, France. The author also thank to David Sibeck of NGFC-NASA, Bob Clauer of VT, and Douglas Staley President of NIA for their continuous supports and insights. The Author also would like to thank Zamala program and Bank of Palestine for supporting my research visits to the US.

## References

- [1] W. Axford. The interaction between the solar wind and the earth's magnetosphere. *J. Geophys. Res.*, 67(10):3791–3796, 1962.
- [2] S. Bale, F. Mozer, and T. Horbury. Density-Transition Scale at Quasiperpendicular Collisionless Shocks. *Phys. Rev. Lett.*, 91(26):265004, Dec. 2003. ISSN 0031-9007. doi: 10.1103/PhysRevLett.91.265004. URL <http://link.aps.org/doi/10.1103/PhysRevLett.91.265004>.
- [3] S. Baraka. *Etude de l'interaction entre le vent solaire et la magnetosphere de la Terre: Modele theorique et Application sur l'analyse de donnees de l'evenement du Halloween d'octobre 2003*. PhD thesis, Universit Pierre et Marie Curie-Paris VI, 2007. URL <https://tel.archives-ouvertes.fr/tel-00138416/en/>.
- [4] S. Baraka and L. Ben-Jaffel. Sensitivity of the Earth's magnetosphere to solar wind activity: Three-dimensional macroparticle model. *Journal of Geophysical Research (Space Physics)*, 112:6212, June 2007. doi: 10.1029/2006JA011946.
- [5] S. Baraka and L. Ben-Jaffel. Impact of solar wind depression on the dayside magnetosphere under northward interplanetary magnetic field. *Annales Geophysicae*, 29:31–46, Jan. 2011. doi: 10.5194/angeo-29-31-2011.
- [6] S. Baraka and L. Jaffel. 3d Simulation of Earth's magnetosphere by Particle-In-Cell and magnetohydrodynamics models: parameteric study. In *AGU Fall Meeting Abstracts*, volume 1, page 4222, 2014.
- [7] S. Baraka, L. Jaffel, and I. Dandouras. The unusual event of Jan 21st 2005 observed by Cluster spacecrafts is considered for comparison by PIC EM Relativistic code simulation. In *AGU Fall Meeting Abstracts*, volume 1, page 2236, 2013.
- [8] L. Ben-Jaffel and G. E. Ballester. Transit of exomoon plasma tori: new diagnosis. *The Astrophysical Journal Letters*, 785(2):L30, 2014.
- [9] L. Ben-Jaffel, M. Strumik, R. Ratkiewicz, and J. Grygorczuk. The Existence and Nature of the Interstellar Bow Shock. *apj*, 779:130, Dec. 2013. doi: 10.1088/0004-637X/779/2/130.
- [10] C. K. Birdsall and A. B. Langdon. *Plasma Physics Via Computer Simulation*. CRC Press, 2005.
- [11] C. Bonifazi and G. Moreno. Reflected and diffuse ions backstreaming from the Earth's bow shock 2. Origin. *Journal of Geophysical Research: Space Physics (1978-2012)*, 86(A6):4405–4413, 1981.
- [12] O. Buneman. Computer space plasma physics. *Simulation Techniques and Software*, page 67, 1993.
- [13] O. Buneman, C. Barnes, J. Green, and D. Nielsen. Principles and capabilities of 3-D, EM particle simulations. *J. Comput. Phys.*, 38(1):1–44, 1980.
- [14] O. Buneman, T. Neubert, and K.-I. Nishikawa. Solar wind-magnetosphere interaction as simulated by a 3-D EM particle code. *Plasma Science, IEEE Transactions on*, 20(6):810–816, 1992.

- [15] O. Buneman, K.-I. Nishikawa, and T. Neubert. Solar Wind-Magnetosphere Interaction as Simulated by a 3d, Em Particle Code. *Space Plasmas: Coupling Between Small and Medium Scale Processes*, pages 347–356, 1995.
- [16] A. Bykov and R. Treumann. Fundamentals of collisionless shocks for astrophysical application, 2. relativistic shocks. *The Astronomy and Astrophysics Review*, 19(1):1–67, 2011.
- [17] J. Behner, C. Dum, and M. Scholer. *Space plasma simulation*, volume 615. Springer, 2003.
- [18] D. Cai, Y. Li, K.-I. Nishikawa, C. Xiao, X. Yan, and Z. Pu. Parallel 3-d electromagnetic particle code using high performance fortran: Parallel tristan. In *Space Plasma Simulation*, pages 25–53. Springer, 2003.
- [19] D. Cai, X. Yan, K.-I. Nishikawa, and B. Lembge. Particle entry into the inner magnetosphere during duskward IMF By: Global three-dimensional electromagnetic full particle simulations. *Geophys. Res. Lett.*, 33(12), 2006.
- [20] D. Cai, A. Esmaili, B. Lembège, and K.-I. Nishikawa. Cusp dynamics under northward imf using three-dimensional global particle-in-cell simulations. *Journal of Geophysical Research: Space Physics*, 120(10):8368–8386, 2015.
- [21] S. Chapman and V. C. A. Ferraro. A New Theory of Magnetic Storms. *nat*, 126:129–130, July 1930. doi: 10.1038/126129a0.
- [22] A. Dmitriev, J. Chao, and D. Wu. Comparative study of bow shock models using Wind and Geotail observations. *J. Geophys. Res.*, 108(A12):1464, 2003.
- [23] J. Dungey. The interplanetary field and auroral theory. *Journal of the Physical Society of Japan Supplement*, 17:15, 1962.
- [24] D. C. Ellison, J. Giacalone, D. Burgess, and S. Schwartz. Simulations of particle acceleration in parallel shocks: Direct comparison between Monte Carlo and one-dimensional hybrid codes. *Journal of Geophysical Research: Space Physics (19782012)*, 98(A12):21085–21093, 1993.
- [25] P. C. Filbert and P. J. Kellogg. Electrostatic noise at the plasma frequency beyond the earth’s bow shock. *jgr*, 84:1369–1381, Apr. 1979. doi: 10.1029/JA084iA04p01369.
- [26] R. J. Fitzenreiter, A. J. Klimas, and J. D. Scudder. Detection of bump-on-tail reduced electron velocity distributions at the electron foreshock boundary. *grl*, 11:496–499, May 1984. doi: 10.1029/GL011i005p00496.
- [27] D. Fontaine, L. Turc, and P. Savoini. Multipoint observations and simulation of the effects of Earth’s bow shock on magnetic clouds’ structure and geoeffectiveness. In *EGU General Assembly Conference Abstracts*, volume 17, page 5908, 2015. URL <http://adsabs.harvard.edu/abs/2015EGUGA...17.5908F>.
- [28] T. Gombosi, D. D. Zeeuw, and C. Groth. Global MHD modeling of space weather. *IEEE Trans, Plasma Sci.*, *ldots*, 2000. URL [http://scholar.google.com/scholar?hl=en&q=T.+I.+Gombosi%2C+D.+L.+De+Zeeuw%2C+C.+P.+T.+Groth%2C+K.+G.+Powell%2C+A.+J.+Ridley%2C+and+P.+Song%2C+%E2%80%9CGlobal+MHD+modeling+of+space+weather%2C%E2%80%9D+IEEE+Trans.+Plasma+Sci.%2C+2000&btnG=&as\\_sdt=1%2C5&as\\_sdtp=#0](http://scholar.google.com/scholar?hl=en&q=T.+I.+Gombosi%2C+D.+L.+De+Zeeuw%2C+C.+P.+T.+Groth%2C+K.+G.+Powell%2C+A.+J.+Ridley%2C+and+P.+Song%2C+%E2%80%9CGlobal+MHD+modeling+of+space+weather%2C%E2%80%9D+IEEE+Trans.+Plasma+Sci.%2C+2000&btnG=&as_sdt=1%2C5&as_sdtp=#0).

- [29] P. Janhunen, M. Palmroth, T. Laitinen, I. Honkonen, L. Juusola, G. Facsko, and T. Pulkkinen. The GUMICS-4 global MHD magnetosphere-ionosphere coupling simulation. *Journal of Atmospheric and Solar-Terrestrial Physics*, 80:48–59, 2012.
- [30] K. Jelnek, Z. Nmeek, J. afrnkov, J.-H. Shue, A. V. Suvorova, and D. G. Sibeck. Thin magnetosheath as a consequence of the magnetopause deformation: THEMIS observations. *Journal of Geophysical Research (Space Physics)*, 115:10203, 2010. ISSN 0148-0227. URL <http://adsabs.harvard.edu/abs/2010JGRA...11510203J>.
- [31] K. Keika, R. Nakamura, W. Baumjohann, V. Angelopoulos, K. Kabin, K. H. Glassmeier, D. G. Sibeck, W. Magnes, H. U. Auster, K. H. Fornacon, J. P. McFadden, C. W. Carlson, E. A. Lucek, C. M. Carr, I. Dandouras, and R. Rankin. Deformation and evolution of solar wind discontinuities through their interactions with the Earth’s bow shock. *Journal of Geophysical Research (Space Physics)*, 114, 2009. ISSN 0148-0227. URL <http://adsabs.harvard.edu/abs/2009JGRA...114.0C26K>.
- [32] P. J. Kellogg. Flow of plasma around the earth. *Journal of Geophysical Research*, 67(10):3805–3811, 1962.
- [33] G. Kowal, E. d. G. Dal Pino, and A. Lazarian. Magnetohydrodynamic simulations of reconnection and particle acceleration: three-dimensional effects. *The Astrophysical Journal*, 735(2):102, 2011.
- [34] V. Krasnoselskikh, M. Balikhin, S. N. Walker, S. Schwartz, D. Sundkvist, V. Lobzin, M. Gedalin, S. D. Bale, F. Mozer, J. Soucek, Y. Hobara, and H. Comisel. The Dynamic Quasiperpendicular Shock: Cluster Discoveries. *Space Sci. Rev.*, 178(2-4):535–598, Mar. 2013. ISSN 0038-6308. doi: 10.1007/s11214-013-9972-y. URL <http://link.springer.com/10.1007/s11214-013-9972-y>.
- [35] E. Kronberg, R. Buk, S. Haaland, B. Klecker, K. Keika, M. Desai, P. Daly, M. Yamauchi, R. Gmez-Herrero, and A. Lui. On the origin of the energetic ion events measured upstream of the Earth’s bow shock by STEREO, Cluster, and Geotail. *Journal of Geophysical Research: Space Physics (19782012)*, 116(A2), 2011.
- [36] A. Kullen, P. Janhunen, and others. Relation of polar auroral arcs to magnetotail twisting and IMF rotation: A systematic MHD simulation study. In *Annales Geophysicae*, volume 22, pages 951–970, 2004.
- [37] J. Leboeuf, T. Tajima, C. F. Kennel, and J. Dawson. Global simulation of the time-dependent magnetosphere. *Geophys. Res. Lett.*, 5(7):609–612, 1978.
- [38] E. Lindman. Free-space boundary conditions for the time dependent wave equation. *J. Comput. Phys.*, 18(1):66–78, 1975.
- [39] I. Mann, D. Milling, I. Rae, L. Ozeke, A. Kale, Z. Kale, K. Murphy, A. Parent, M. Usanova, D. Pahud, et al. The upgraded carisma magnetometer array in the themis era. *Space Science Reviews*, 141(1-4):413–451, 2008.
- [40] N. C. Maynard, C. J. Farrugia, W. J. Burke, D. M. Ober, J. D. Scudder, F. S. Mozer, C. T. Russell, H. Rme, C. Mouikis, and K. D. Siebert. Interactions of the heliospheric current and plasma sheets with the bow shock: Cluster and Polar observations in the magnetosheath. *Journal of Geophysical Research: Space Physics (19782012)*, 116(A1), 2011.

- [41] K. Meziane, M. Wilber, A. Hamza, C. Mazelle, G. Parks, H. Reme, and E. Lucek. Evidence for a high-energy tail associated with foreshock field-aligned beams. *J. Geophys. Res.*, 112(A1):A01101, 2007.
- [42] K. Meziane, A. M. Hamza, M. Maksimovic, and T. Y. Alrefay. The Earth’s bow shock velocity distribution function. *Journal of Geophysical Research: Space Physics*, 120(2):1229–1237, 2015. URL <http://onlinelibrary.wiley.com/doi/10.1002/2014JA020772/pdf>.
- [43] T. Moritaka, Y. Kajimura, H. Usui, M. Matsumoto, T. Matsui, and I. Shinohara. Momentum transfer of solar wind plasma in a kinetic scale magnetosphere. *Physics of Plasmas (1994-present)*, 19(3):032111, 2012.
- [44] K.-I. Nishikawa. Particle entry into the magnetosphere with a southward interplanetary magnetic field studied by a three-dimensional electromagnetic particle code. *Journal of Geophysical Research: Space Physics (19782012)*, 102(A8):17631–17641, 1997.
- [45] N. Omidi, X. Blanco-Cano, and C. Russell. Macrostructure of collisionless bow shocks: 1. Scale lengths. *Journal of Geophysical Research: Space Physics (19782012)*, 110(A12), 2005.
- [46] N. Omidi, D. Sibeck, X. Blanco-Cano, D. Rojas-Castillo, D. Turner, H. Zhang, and P. Kajdi. Dynamics of the foreshock compressional boundary and its connection to foreshock cavities. *Journal of Geophysical Research (Space Physics)*, 118:823–831, 2013. ISSN 0148-0227. URL <http://adsabs.harvard.edu/abs/2013JGRA...118..823O>.
- [47] M. Palmroth, T. Pulkkinen, P. Janhunen, and C.-C. Wu. Stormtime energy transfer in global MHD simulation. *J. Geophys. Res.*, 108(A1):SMP24–1, 2002.
- [48] M. Palmroth, P. Janhunen, T. Pulkkinen, A. Aksnes, G. Lu, N. stgaard, J. Watermann, G. Reeves, and G. Germany. Assessment of ionospheric Joule heating by GUMICS-4 MHD simulation, AMIE, and satellite-based statistics: towards a synthesis. In *Annales Geophysicae*, volume 23, pages 2051–2068. Copernicus GmbH, 2005.
- [49] G. K. Parks. Why space physics needs to go beyond the MHD box. *Space science reviews*, 113(1-2):97–121, 2004.
- [50] G. Paschmann, N. Sckopke, I. Papamastorakis, J. Asbridge, S. Bame, and J. Gosling. Characteristics of reflected and diffuse ions upstream from the earth’s bow shock. *Journal of Geophysical Research: Space Physics (19782012)*, 86(A6):4355–4364, 1981.
- [51] M. Peredo, J. Slavin, E. Mazur, and S. Curtis. Three-dimensional position and shape of the bow shock and their variation with Alfvénic, sonic and magnetosonic Mach numbers and interplanetary magnetic field orientation. *Journal of Geophysical Research: Space Physics (19782012)*, 100(A5):7907–7916, 1995.
- [52] A. Petrukovich, A. Artemyev, I. Vasko, R. Nakamura, and L. Zelenyi. Current sheets in the earth magnetotail: Plasma and magnetic field structure with cluster project observations. *Space Science Reviews*, 188(1-4):311–337, 2015.
- [53] D. Pokhotelov, S. von Althaus, Y. Kempf, R. Vainio, H. Koskinen, and M. Palmroth. Ion distributions upstream and downstream of the Earth’s bow shock: first results from Vlasiator. In *Annales Geophysicae*, volume 31, pages 2207–2212. Copernicus GmbH, 2013.
- [54] P. L. Pritchett. Particle-in-cell simulations of magnetosphere electrodynamics. *Plasma Science, IEEE Transactions on*, 28(6):1976–1990, 2000.

- [55] D. Rojas-Castillo, X. Blanco-Cano, P. Kajdi, and N. Omidi. Foreshock compressional boundaries observed by Cluster. *Journal of Geophysical Research: Space Physics*, 2013.
- [56] A. A. Samsonov. Specific features of magnetic barrier formation near the magnetopause. *Geomagnetism and Aeronomy*, 47:316–324, June 2007. doi: 10.1134/S0016793207030061.
- [57] P. Savoini, B. Lembege, and J. Stienlet. On the origin of the quasi-perpendicular ion foreshock: Full-particle simulations. *Journal of Geophysical Research (Space Physics)*, 118: 1132–1145, Mar. 2013. doi: 10.1002/jgra.50158.
- [58] C. Schreiner and F. Spanier. Wave-particle-interaction in kinetic plasmas. *Comput. Phys. Commun.*, 2014.
- [59] Y. Seki, M. Nishino, M. Fujimoto, Y. Miyashita, K. Keika, H. Hasegawa, K. Okabe, Y. Kasaba, T. Terasawa, T. Yamamoto, and others. Observations of loss coneshaped back streaming energetic protons upstream of the Earth’s bow shock. *Journal of Geophysical Research: Space Physics (19782012)*, 114(A11), 2009.
- [60] I. Shaikhislamov, V. Antonov, Y. P. Zakharov, E. Boyarintsev, A. Melekhov, V. Posukh, and A. Ponomarenko. Small scale magnetosphere: Laboratory experiment, physical model and Hall MHD simulation. *arXiv preprint arXiv:1110.4461*, 2011.
- [61] R. Treumann. Fundamentals of collisionless shocks for astrophysical application, 1. Non-relativistic shocks. *The Astronomy and Astrophysics Review*, 17(4):409–535, 2009.
- [62] A. Vapirev, G. Lapenta, A. Divin, S. Markidis, P. Henri, M. Goldman, and D. Newman. Formation of a transient front structure near reconnection point in 3-D PIC simulations. *Journal of Geophysical Research: Space Physics*, 2013.
- [63] J. Villasenor and O. Buneman. Rigorous charge conservation for local electromagnetic field solvers. *Comput. Phys. Commun.*, 69(2):306–316, 1992.
- [64] D. Welling, M. Liemohn, G. Toth, and A. Glocher. Evaluating the Importance of Outflow Velocity at the MHD Inner Boundary. In *AGU Fall Meeting Abstracts*, volume 1, page 2105, 2013.
- [65] R. Winglee, W. Lewis, and G. Lu. Mapping of the heavy ion outflows as seen by IMAGE and multifluid global modeling for the 17 April 2002 storm. *Journal of Geophysical Research: Space Physics (19782012)*, 110(A12), 2005.
- [66] E. Wodnicka. On a magnetosphere disturbed by solar wind; observations of macroelectrons. In *Annales Geophysicae*, volume 27, pages 2331–2339. Copernicus GmbH, 2009.

## 7 Tables

Parameters	PIC code	GUMICS-v4
CPU time	50 Min	5 Hours
Machine	Single processor PC	CCMC-Super Computer
Ionosphere	No	Yes
Grid Cell	Fixed	Adaptive
Grid size	$1R_E^3$	$(0.1 - 8R_E)^3$
Small Box Size	$155 \times 105 \times 105R_E$	$250 \times 130 \times 130R_E$
$\rho$	$0.8 \frac{N}{\Delta^3}$	$5.0cm^{-3}$
$B_z(x)$	0.2	$6.5(nT)$
$V_x(x)$	0.25	$500 (km.sec^{-1})$
$V_A$	0.028	$63(km.sec^{-1})$
<u>Unitless values</u>		
$\frac{V_A}{V_{sw}}$	0.11	0.12
$M_A$	8.9	7.8
$M_{MS}$	5.5	5.2
$\beta$	1.6	2.7

Table 1: shows the solar wind input scaled parameters for the **PIC** and their corresponding values for the **MHD** code

## 8 Figures

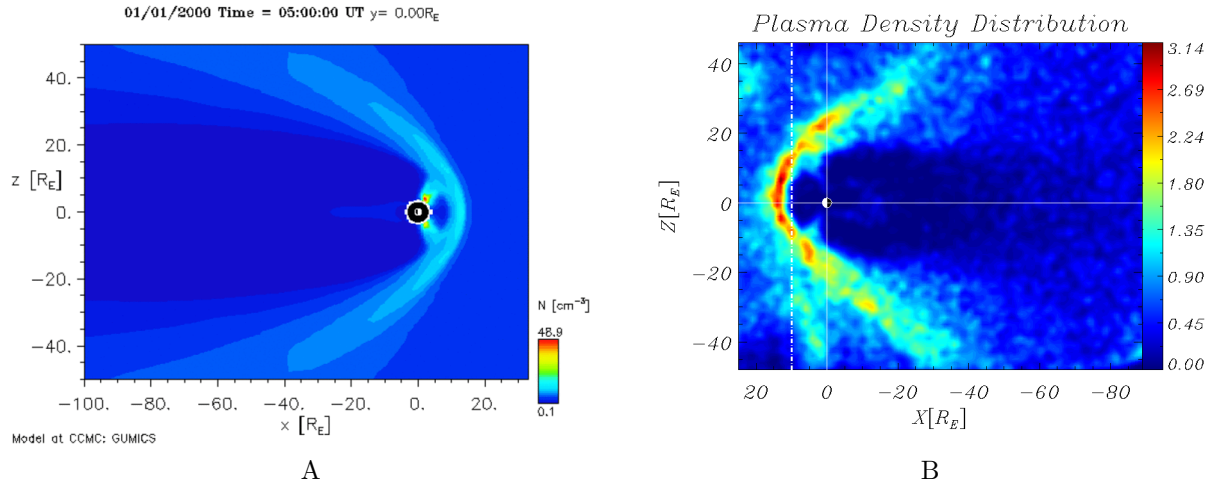


Figure 1: Plasma density distribution in Noon-Midnight axis. Panel A shows the MHD system generated plasma distribution, while panel B shows the plasma distribution as simulated by PIC code

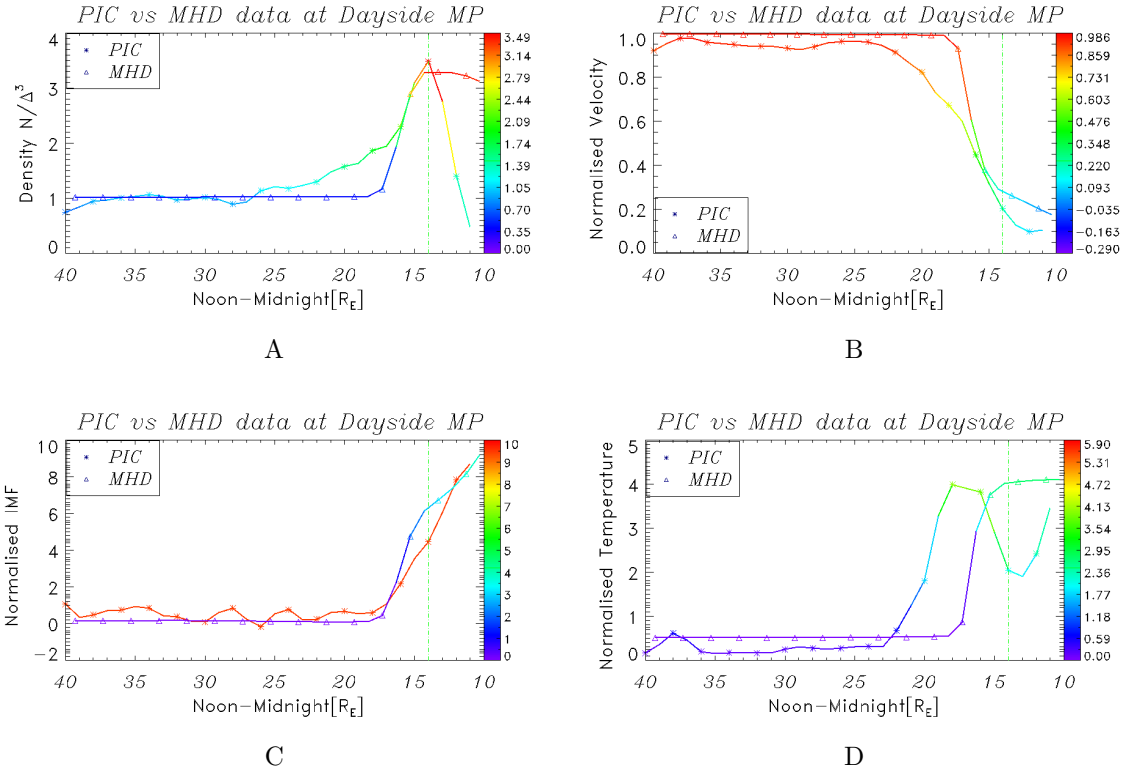


Figure 2: Colored Elevated plasma parameters plotted in nose direction. In frame (A) density profile multi-plot is shown in the dayside magnetosphere as simulated by PIC code ( $\star$  symbol) and MHD ( $\triangle$  symbol). Similarly, Velocity, IMF and Temperature is depicted in Frames (B), (C) and (D) respectively. All parameters are normalized to their input values. Units are in  $R_E$ .

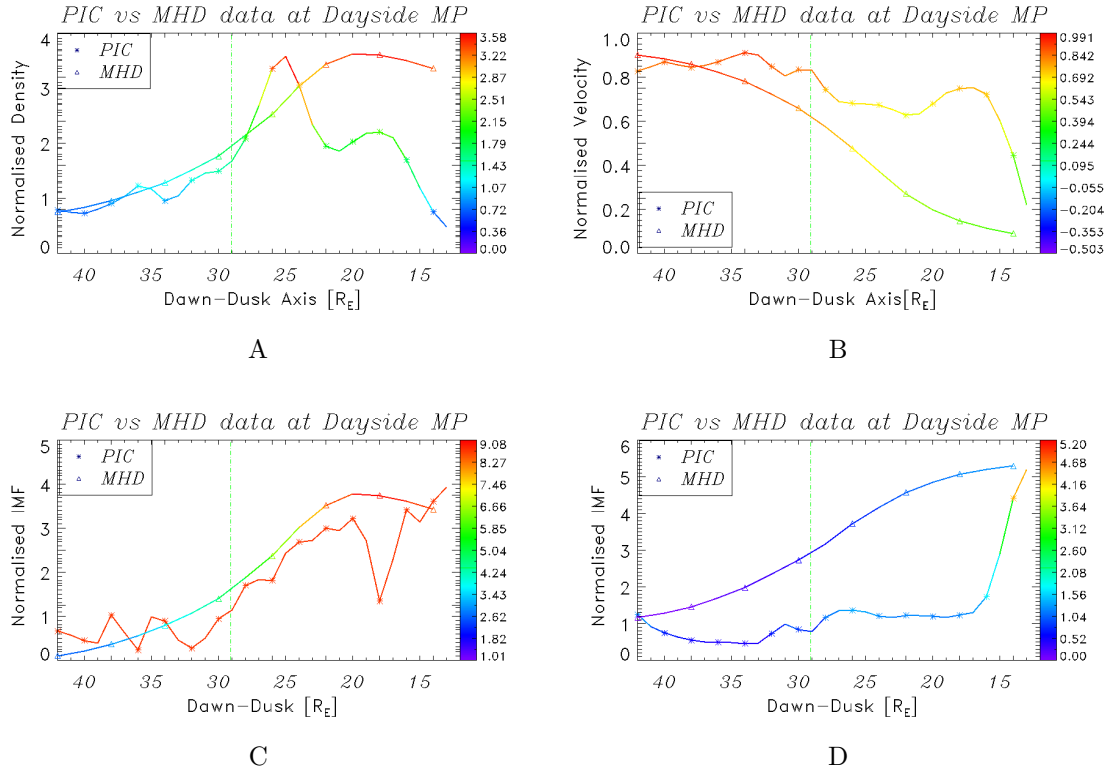
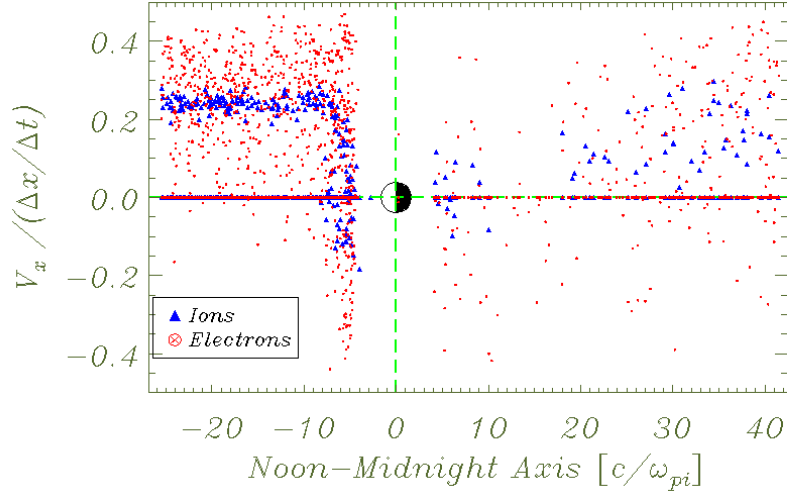


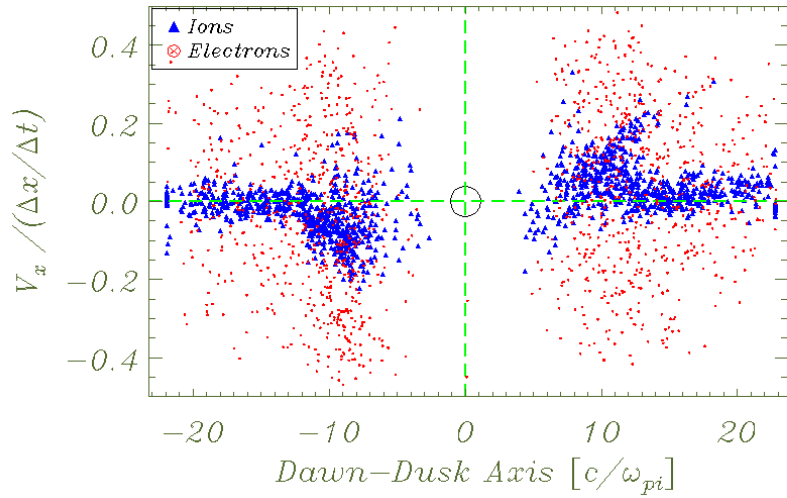
Figure 3: Colored Elevated plasma parameters plotted in the dusk direction. In frame (A) density profile multi-plot is shown in the dayside magnetosphere as simulated by PIC code ( $\star$  symbol) and MHD ( $\triangle$  symbol). Similarly, Velocity, IMF and Temperature is depicted in Frames (B), (C) and (D) respectively. All parameters are normalized to their input values. Units are in  $R_E$ .

*Electron and Ion Spatial Distribution*



**A**

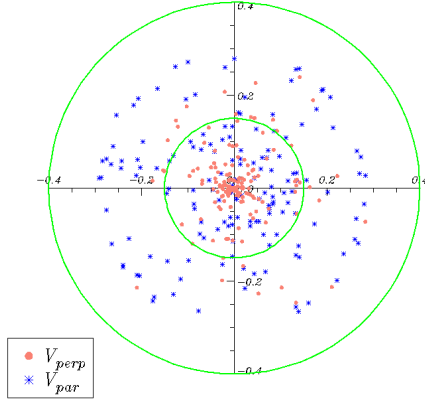
*Electron and Ion Spatial Distribution*



**B**

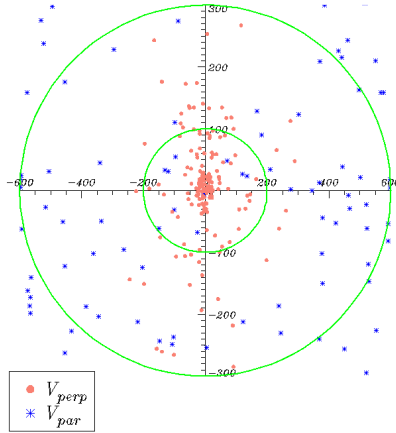
Figure 4: In panel (A) spatial distribution of ions and electrons velocities taken at nose direction both in day and night side of the magnetosphere. The thermal behavior of electrons can be clearly seen in this figure, especially at the day side portion of the magnetosphere. In panel (B), the same spatial distribution but is taken in the dusk direction

*PIC Polar velocity distribution*



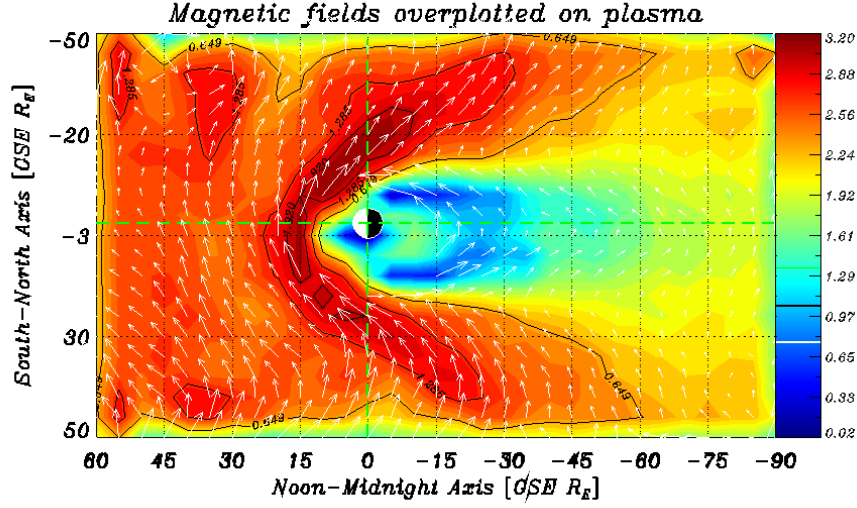
**A**

*MHD Polar velocity distribution*

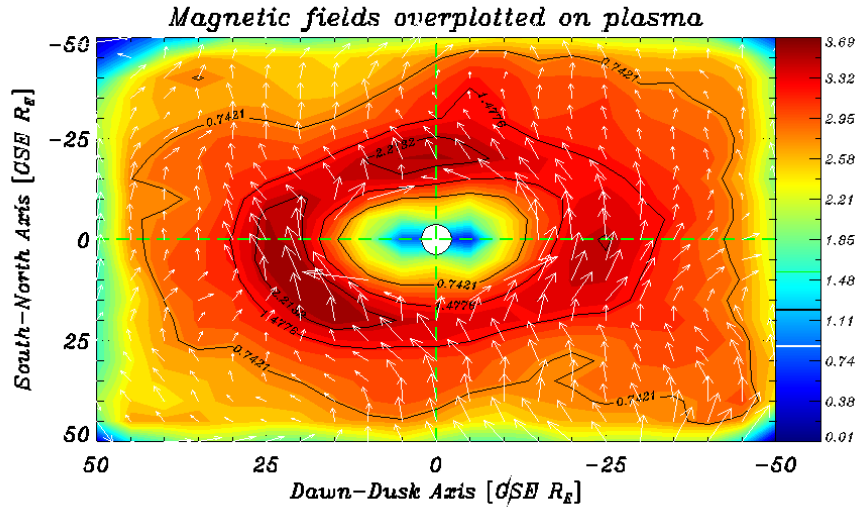


**B**

Figure 5: Panel A shows the polar distribution of parallel and perpendicular velocities as generated by PIC code (input value is  $0.25 \equiv 500 \text{ km}\cdot\text{sec}^{-1}$ ). Panel B shows same distribution as simulated by MHD code (input solar wind value is  $500 \text{ km}\cdot\text{sec}^{-1}$ )



A



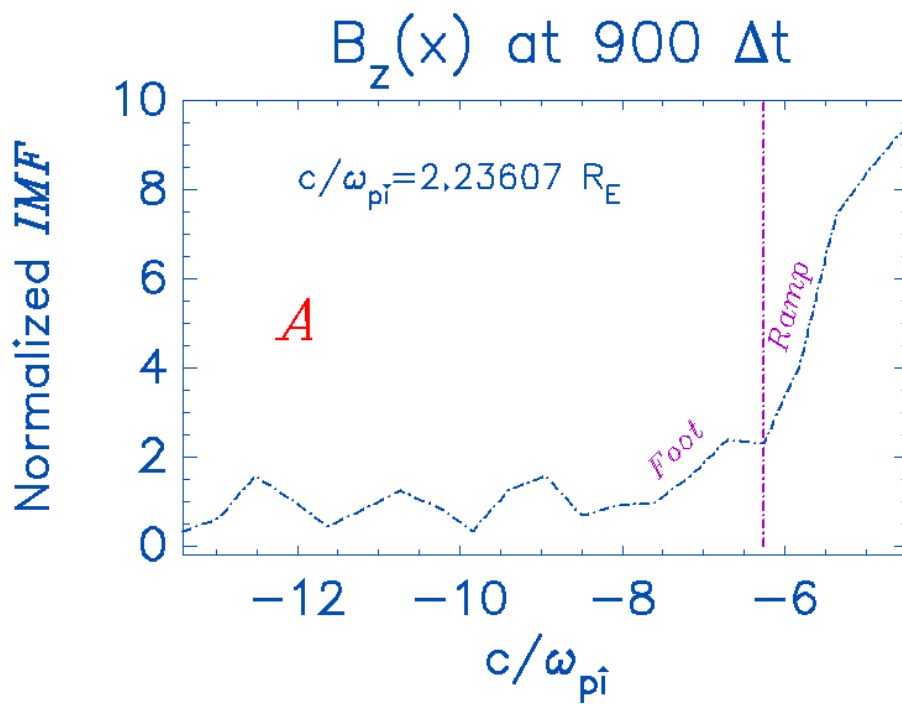


Figure 7: shows the  $B_z(x)$  structure at the bow shock/foreshock region.  $B_z(x)$  as simulated by PIC code clearly depict the foot and ramp structure, compared with the theoretical model reported in<sup>61</sup> in Fig 10.

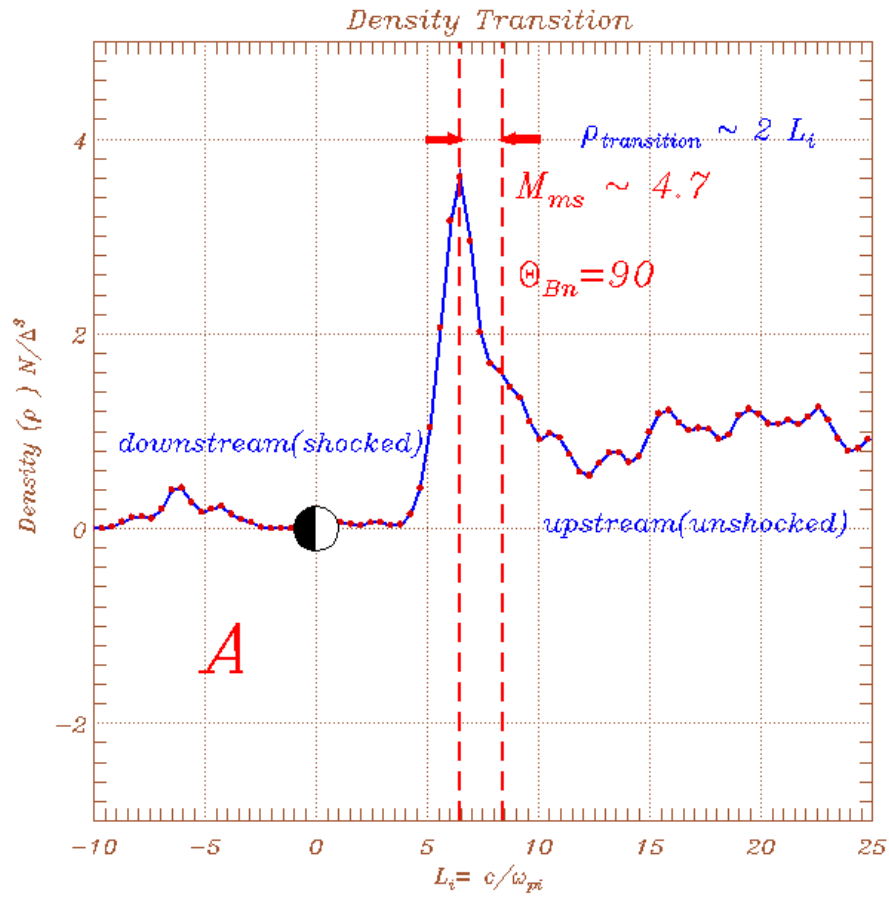


Figure 8: shows the density transition between downstream (shocked) and upstream (unshocked) as simulated by our code, the red vertical lines show the density transition scale. The figure is mirrored for comparison purposes. Our result is compared with cluster data density transition scale as reported by<sup>2</sup> in Fig 5.4